Reexamination of Chirped Pulse Control of Wave Packet Motion in NaI

Hui Tang and Stuart A. Rice*

The James Franck Institute, The University of Chicago, Chicago, Illinois 60637

Received: July 29, 1997; In Final Form: September 23, 1997[⊗]

Recent experimental and theoretical studies of femtosecond pump−probe pulse excitation of NaI have led to information concerning bound-state wave packet motion, the control of wave packet localization, and the control of the branching between photodissociation products. This paper reports calculations that (i) resolve the discrepancy between the experiments that employ 50−60 fs pulses and those that employ 150−175 fs pulses; the former experiments show that the wave packet motion changes from simple periodic to multiple periodic and back to simple periodic in a time span of 40 ps, while the latter experiments do not show this change in wave packet dynamics; (ii) examine the relationship between pulse width and photodissociation yield; and (iii) determine the optimal nonlinear chirped pump pulse that best localizes the excited-state wave packet with prescribed position and momentum chosen to enhance the photodissociation yield.

I. Introduction

As a result of recent experimental and theoretical studies,[1−15] NaI has become a vehicle for studying bound-state wave packet motion, the control of wave packet localization, and the control of the branching between photodissociation products. The relevant potential energy curves are displayed in Figure 1. As in all of the alkali halide molecules, the X $^1\Sigma_0^-$ (ionic) ground-state potential energy curve crosses that of the A (covalent) electronic excited state. If there were no interaction between these states, the ground electronic state would dissociate to form the ions Na^+ and I^-, while the first electronic excited state would dissociate to form the atoms Na ($^2S_{1/2}$) and I ($^2P_{3/2}$). In fact, there is strong coupling between the X and A states and, since the asymptotic state with product species Na^+ and I^- has much higher energy than the asymptotic state with product species Na ($^2S_{1/2}$) and I ($^2P_{3/2}$), a potential well is formed in the resultant adiabatic excited state.

In the several experimental studies reported,[1−6] a short laser pulse is used to pump ground-state NaI to the first excited state via the X → A transition. The oscillatory motion of the wave packet formed on the excited-state potential energy surface is then followed by applying, after a time delay, another short probe pulse, which generates a state that dissociates into Na (^2P) and I. The total Na (^2P) emission induced by the second pulse gives information about the character of the excited-state wave packet at the time when a photon from probe pulse was absorbed. Alternatively, the delayed second pulse can be used to generate Na^+ and I. The experimental data consist of measurements of the dependence on the time delay between the pump and probe pulses of either the laser-induced fluorescence (LIF) signal or the sodium ion and photoelectron signals. When LIF detection is used and the probe pulse central frequency is resonant with the sodium D line, it is found that there are sudden very nearly periodic jumps in the signal intensity, between which the signal is sensibly constant. The increases in the LIF signal occur when the NaI separation on the excited-state potential energy surface reaches R_x, the point at which the ionic and covalent potential energy curves cross, predissociation takes place, and the product Na atom is excited by the probe pulse. If the probe pulse central frequency is not resonant with the sodium D line, the LIF signal as a function of delay time displays oscillations with an amplitude that decreases as the time delay increases; the frequency of the oscillations is the same as the vibrational frequency on the upper adiabatic state at the energy reached by the pump laser. When sodium ion and photoelectron detection is used, it is found that the Na^+ ions are formed when the wave packet reaches R_x and that NaI^+ and Na^+ are generated in phase, with no measurable photoionization signal from wave packets on the portion of the A state potential energy curve with $R < R_x$. Although there is, in general, agreement between the experimental studies using the two detection methods, they disagree concerning the character of the time dependence of the wave packet dynamics on the portion of the A-state potential energy curve with $R < R_x$. The experiments[2] that employ LIF detection and use 50−60 fs pulses, show that the wave packet motion changes from simple periodic to multiple periodic back to simple periodic in a time span of 40 ps; those[5] that employ sodium ion and photoelectron detection, and use 150−175 fs pulses, do not show this change in wave packet dynamics. One of the purposes of this short paper is to resolve this discrepancy.

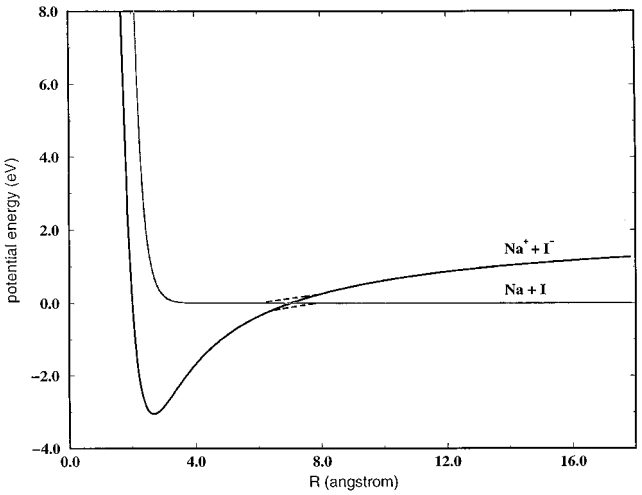

Figure 1. Potential energy surfaces for NaI. The potential parameters can be found in ref 7.

Engel and Metiu[7] were among the first to report a detailed quantum mechanical analysis of the experiments described above. Their calculations, based on first-order perturbation theory, captured all of the essential features of the experimental results except for the finding that NaI^+ and Na^+ are generated

[⊗] Abstract published in *Advance ACS Abstracts,* December 1, 1997.

S1089-5639(97)02488-2 CCC: $14.00

in phase (they predict the generation of these ions to be out of phase). Braun, Meier, and Engel[15] have calculated the time evolution of the photoelectron spectrum of NaI and have predicted that a high-energy electron is emitted at the outer turning point, R_x, and a low-energy electron at the inner turning point, of the wave packet motion on the A-state potential energy curve. The former prediction agrees with the experimental data, whereas the latter does not. This discrepancy, which likely has the same origin as that concerning the in-phase generation of NaI^+ and Na^+, namely, inadequate treatment of the separation dependence of the ionization cross section and the transition dipole moment, is not further discussed in this paper.

NaI has also been used as a vehicle to study the influence of pulse shaping on the wave packet dynamics. In particular, it has been demonstrated[14] that a chirped pump pulse can be used to control the localization of a vibrational wave packet on an excited-state potential energy surface. That is, subject only to the restrictions imposed by the uncertainty principle, a wave packet can be forced to have a specified position and internuclear momentum at a specified time. Then it is to be expected that a properly localized wave packet can be used to generate more product Na (^{2}P) than can be obtained without localization. Bardeen et al.[14] have reported experimental and theoretical studies of the use of linear chirped pulses to localize a wave packet on the A-state potential energy surface of NaI and thereby to control the ratio of yields of Na (^{2}P) to Na (^{2}S). In this note we reexamine which positive or negative linear chirp, and which nonlinear chirp, optimizes the formation of Na (^{2}P) in the two-pulse pump−probe photodissociation of NaI. We also relate the use of chirped pulses to the generic control scheme of Tang, Kosloff, and Rice[16] and examine what can be learned from a frequency space examination of chirped pulse control.

II. General Remarks

A. Calculation Details. Unlike Engel and Metiu,[7] we do not use perturbation theory to analyze the wave packet dynamics. Using the ground-state and first excited-state wave functions as a basis, the time-dependent molecular Hamiltonian can be represented in the form

$$H(t) = \begin{pmatrix} T + V_1 & V_{12} - \mu E(t) \\ V_{12} - \mu \mathrm{E}(t) & T + V_2 \end{pmatrix} \tag{1}$$

where V_{12} is the coupling between the two states, μ is the transition dipole moment, and $E(t)$ is the applied electric field. Since the exact form of the transition dipole moment is unknown, we adopt the Condon approximation. We assume that the unchirped pump laser pulse has a Gaussian temporal envelope,

$$E(t;\omega) = E_0 \cos(\omega(t - t_0)) \exp\left(-\frac{(t - t_0)^2}{2\sigma^2}\right) \tag{2}$$

where ω is the pulse carrier frequency, and that the linearly chirped pulse has the form[17]

$$E(t;\omega,\alpha) = E_0 \cos(\omega(t - t_0) + \alpha(t - t_0)^2) \exp\left(-\frac{(t - t_0)^2}{2\sigma^2}\right) \tag{3}$$

where α is the linear chirp rate. We note that the power spectrum of the pulse broadens as the magnitude of α increases. Our calculational scheme is based on analytic diagonalization of the 2×2 potential energy matrix

$$V(t) = \begin{pmatrix} V_1 & V_{12} - \mu E(t) \\ V_{12} - \mu E(t) & V_2 \end{pmatrix} \tag{4}$$

with the propagation of the wave packet calculated using the split operator scheme.[18,19] In this scheme we use $e^{V(t)} = Te^{V_D(t)}T^+$, where T is the matrix that diagonalizes $V(t)$, $V(t) = TV_D(t)T^+$, and T^+ is the Hermitian conjugate of T. Since the potential energy matrix $V(t)$ must be diagonized at every time step, having an analytic expression for T greatly expedites the diagonization process. Various integration time steps have been employed to carefully test the convergence of numerical outcome, which shows the adopted scheme is stable for the present system.

Following Engel and Metiu, we do not calculate the LIF signal directly; rather, we assume that the LIF signal is proportional to the cumulative flux of wave packet amplitude that passes through R_x, since the free sodium atom wave packet never returns to R_x once it crosses this point on the excited-state potential energy surface. The flux is defined by

$$j(R,t) = \frac{\hbar}{2im}\left[\psi^* \frac{\mathrm{d}\psi}{\mathrm{d}R} - \frac{\mathrm{d}\psi^*}{\mathrm{d}R}\psi\right] \tag{5}$$

where m is the reduced mass of NaI and the cumulative flux is determined from

$$J_f(R_0,t) = \int_0^t j(R_0,\tau)\, \mathrm{d}\tau \tag{6}$$

where R_0 is any separation greater than R_x. To calculate the derivative in (5) we expand $\psi(R)$ in a basis of sine functions,

$$\psi(R) = \sqrt{\frac{2}{L}} \sum_n C_n \sin\frac{n\pi R}{L} \tag{7}$$

whereupon

$$\left.\frac{\mathrm{d}\psi(R)}{\mathrm{d}R}\right|_{R=R_0} = \sqrt{\frac{2}{L}} \sum_n C_n \frac{n\pi}{L} \cos\left(\frac{n\pi R}{L}\right)\Bigg|_{R=R_0} \tag{8}$$

with L the total length of the integration grid. Then

$$j(R_0,t) = \frac{\hbar}{m} \mathrm{Im}\left(\psi^* \frac{\mathrm{d}\psi}{\mathrm{d}R}\right)\Bigg|_{R=R_0} \tag{9}$$

When the probe laser pulse is not resonant with the D line of the free Na atom, the measurements detect either the population on the excited-state potential energy surface in the range $R < R_x$ or that on the ground-state potential energy surface in the range $R > R_x$ (See Figure 1). Since the time dependences of these populations are out of phase, we can choose either to monitor the evolution of the system. Our calculations are based on monitoring

$$P_I(t) = \int_{R_x}^{\infty} \mathrm{d}R |\psi_I(R,t)|^2 \tag{10}$$

To calculate the functional form of the chirping required for the best localization of the wave packet, we employ optimum control theory using the Kosloff−Rice−Gaspard−Tersigni-Tannor formulation.[20,21] The control field is obtained from the extremum of the constrained objective functional

$$I = \langle \psi_f | P | \psi_f \rangle + \int_{t_0}^{t_f} \mathrm{d}t \left[\left\langle \Psi \middle| \mathrm{i}\frac{\delta}{\delta t} - H \middle| \psi \right\rangle - \mathrm{c.c.}\right] + \lambda\left[\int_{t_0}^{t_f} \mathrm{d}t \mathbf{E}^2(t) - E\right] \tag{11}$$

where P is the projection operator defining the overlap between

the system wave function and the target wave function, E is the energy fluence of the applied electromagnetic field, and Ψ and λ are Lagrange multipliers for the constraints that the coupled matter−radiation system satisfies the Schroedinger equation and that the energy fluence of the applied field is E, respectively. Equation 11 is solved iteratively.

B. Frequency Domain Representation of Chirped Pulse Control of Dynamics. The influence of pulse chirping on the excitation of a system with two potential energy surfaces is often visualized in terms of the need to shift the pulse frequency to follow the change in separation of these surfaces as the internuclear distance changes.[22−30] In this section we examine a frequency space representation of the influence of pulse chirping on the transfer of energy and population between the two potential energy surfaces. To achieve this end, we use the generic representation of control dynamics proposed by Tang, Kosloff, and Rice.[16] In that work it is shown that the rate of change of energy of the coupled radiation−matter system can be written in the form

$$\frac{\mathrm{d}\langle E\rangle}{\mathrm{d}t} = -2\mathrm{Re}\left\{\langle \mu \otimes S_+\rangle \frac{\partial \mathbf{E}}{\partial t}\right\} \tag{12}$$

where $S_+ = |2\rangle\langle 1|$ is the raising operator for transfer between the two energy surfaces $|1\rangle$ and $|2\rangle$, μ is the transition dipole moment operator, $\langle \mu \otimes S_+\rangle$ is the expectation value of the instantaneous transition dipole moment, and $\mathbf{E}$ is the electric field. Equation 12 states, as expected, that in a unit time interval the energy transfer between the molecule and the field is determined by the instantaneous transition dipole moment and the time derivative of the electric field. The Fourier space counterpart of (12) is obtained as follows. We introduce

$$\langle \mu \otimes S_+\rangle_t = \frac{1}{(2\pi)^{1/2}}\int_{-\infty}^{\infty} \mathrm{d}\omega \langle \mu \otimes S_+\rangle_\omega \mathrm{e}^{-\mathrm{i}\omega t} \tag{13}$$

and

$$\frac{\partial \mathbf{E}}{\partial t} = \frac{1}{(2\pi)^{1/2}}\int_{-\infty}^{\infty} \mathrm{d}\omega(-\mathrm{i}\omega)\, \mathbf{E}(\omega)\mathrm{e}^{-\mathrm{i}\omega t} \tag{14}$$

so that

$$\frac{\mathrm{d}\langle E\rangle}{\mathrm{d}t} = 2\mathrm{Re}\left\{\frac{\mathrm{i}}{2\pi}\int_{-\infty}^{\infty} \mathrm{d}\omega \langle \mu \otimes S_+\rangle_\omega \int_{-\infty}^{\infty} \mathrm{d}\omega'\, \omega' \mathbf{E}(\omega')\mathrm{e}^{\mathrm{i}(\omega+\omega')t}\right\} \tag{15}$$

Let $\Omega = \omega + \omega'$, so that

$$\frac{\mathrm{d}\langle E\rangle}{\mathrm{d}t} = 2\mathrm{Re}\left\{\frac{\mathrm{i}}{2\pi}\int_{-\infty}^{\infty} \mathrm{d}\omega \langle \mu \otimes S_+\rangle_\omega \int_{-\infty}^{\infty} \mathrm{d}\Omega(\Omega-\omega) \times \mathbf{E}(\Omega-\omega)\mathrm{e}^{-\mathrm{i}\Omega t}\right\} \tag{16}$$

Then, integration with respect to t, recognition of the delta function representation $\delta(\Omega) = \delta(-\Omega) = (2\pi)^{-1}\int_{-\infty}^{\infty}\mathrm{d}t\mathrm{e}^{\mathrm{i}\Omega t}$, and using the fact that the electric field is real so $\mathbf{E}(-\omega) = E^*(\omega)$[31]

$$\Delta(\langle E\rangle) = \int_{-\infty}^{\infty}\frac{\mathrm{d}\langle E\rangle}{\mathrm{d}t} = 2\mathrm{Im}\{\int_{-\infty}^{\infty}\mathrm{d}\omega\omega\langle \mu \otimes S_+\rangle_\omega \mathbf{E}^*(\omega)\} \tag{17}$$

or

$$\frac{d\langle E\rangle}{\mathrm{d}\omega} = 2\omega\mathrm{Im}\{\langle \mu \otimes S_+\rangle_\omega \mathbf{E}^*(\omega)\} \tag{18}$$

Equation 18 explicitly shows that in a unit frequency interval the energy transfer between the molecule and the field is dictated by the frequency, the spectrum of instatantaneous dipole moment, and the conjugate of field spectrum.

Similarly, it can be shown that the frequency space representation of the flow of population from the ground state to the excited state,

$$\frac{\mathrm{d}N_\mathrm{g}}{\mathrm{d}t} = -\frac{\mathrm{i}}{\hbar}\langle \mu \otimes (S_+\mathbf{E} - S_-\mathbf{E}^*)\rangle = \frac{2}{\hbar}\mathrm{Im}\{\langle \mu \otimes S_+\rangle \mathbf{E}(\mathrm{t})\} \tag{19}$$

is

$$\frac{\mathrm{d}N_\mathrm{g}}{\mathrm{d}\omega} = \frac{2}{\hbar}\mathrm{Im}\{\langle \mu \otimes S_+\rangle_\omega \mathbf{E}^*(\omega)\} \tag{20}$$

and that the frequency space representation of the flow of energy from the ground state to the excited state is

$$\frac{\mathrm{d}E_\mathrm{g}}{\mathrm{d}\omega} = \frac{2}{\hbar}\mathrm{Im}\{\langle \mu H_\mathrm{g} \otimes S_+\rangle_\omega \mathbf{E}^*(\omega)\} \tag{21}$$

The influence of the chirp on the transfer of population and energy between the potential energy surfaces is now made explicit through the representation

$$\mathbf{E}(\omega) = |\mathbf{E}(\omega)|\mathrm{e}^{\mathrm{i}\Phi t}$$

$$\Phi(\omega) = \Phi(\omega_0) + \Phi'(\omega_0)(\omega-\omega_0) + \frac{1}{2}\Phi''(\omega_0)(\omega-\omega_0)^2 + \ldots \tag{22}$$

in which $\Phi''(\omega_0)$ is the chirp.[30,32] This spectral representation of the model two surface system complements the usual temporal representation.

III. Results

A. Predissociation Dynamics. We have carried out calculations with pump pulses that have full width at half-maximum (fwhm) of 21, 62, and 186 fs. The initial wave packet was taken to be the $v = 0$ vibrational eigenfunction of the ground-state potential energy curve. The central wavelength of the pump pulse was taken to be 329 nm, resonant with the 3s ^{2}S → 3p ^{2}P transition of the Na atom. Despite the avoided crossing between the X and A potential energy surfaces of NaI, the wave packet on the A-state potential energy curve can cross to the X state with a transition probability that is well approximated by the Landau−Zener formula.[33] Consequently, the wave packet executes damped oscillatory motion between the inner and outer turning points of the metastable well on the A-state potential energy curve. Our calculations follow those oscillations for 40 ps, as in the experimental studies.

In Figure 2a, we display $P_\mathrm{I}(t)$ and $J_\mathrm{f}(t)$ when the pump pulse is a Gaussian with fwhm of 21 fs. In this case $P_\mathrm{I}(t)$ exhibits oscillatory behavior from $t = 0$ to $t = 10$ ps with a period of about 982 fs. From $t = 10$ to $t = 17$ ps $P_\mathrm{I}(t)$ has multiple periodic character, whereas from $t = 17$ to $t = 33$ ps there is a recurrence of simple oscillatory behavior with a period about the same as in the time domain $t = 0$ to $t = 10$ ps. The alternation in the structure of the oscillations of $P_\mathrm{I}(t)$ as the time increases has been observed by Zewail and co-workers,[2] who used pump pulses with fwhm of 50−60 fs, but not by Jouvet and co-workers,[5] who used pump pulses with fwhm of 150−300 fs. The behavior observed by Zewail and co-workers is that expected when the initial wave packet on the excited-state potential energy surface is spatially localized and has a spectral

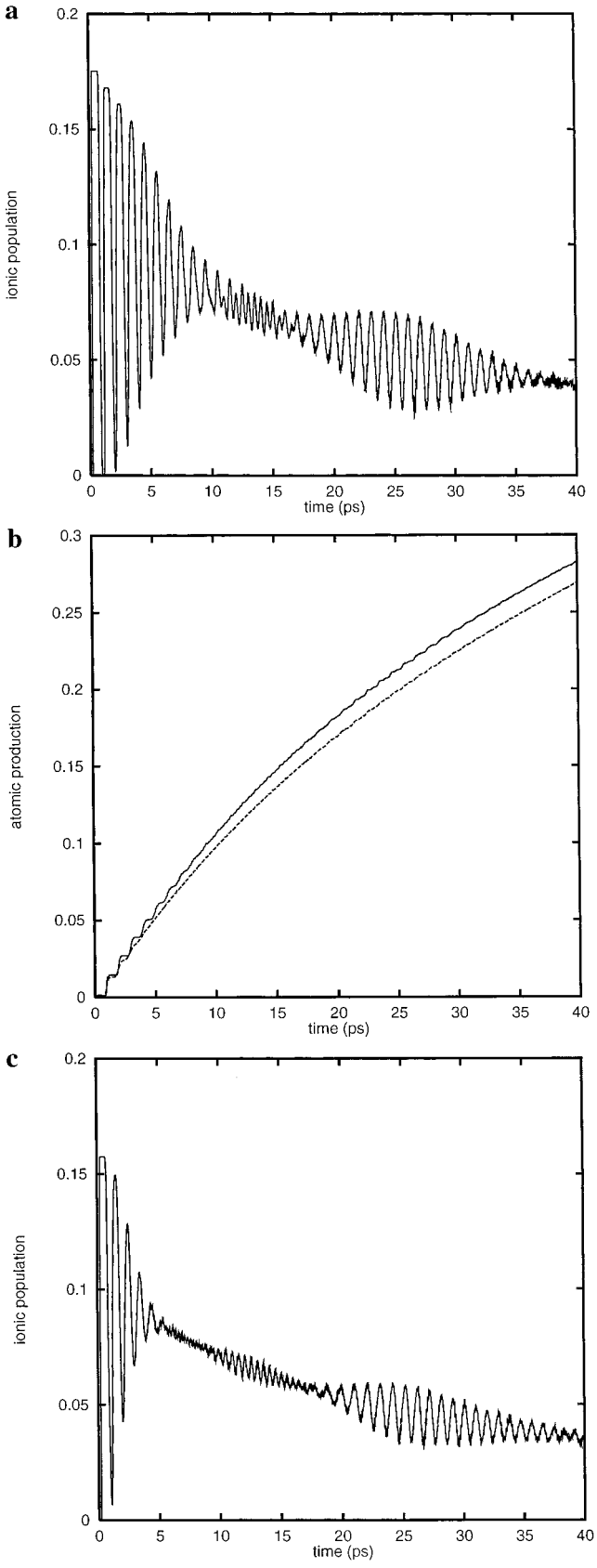

Figure 2. (a) Ionic-state population $P_I(t)$ created by an unchirped pulse of width 21 fs. (b) Atomic production $J_f(t)$ for both unchirped and chirped pulses of width 21 fs. The solid line is for the unchirped pulse; the dashed line for chirped pulse with $\alpha = 5 \times 10^{-6}$. (c) Ionic-state population created by a chirped pulse with $\alpha = 5 \times 10^{-6}$.

content that spans the vibrational states of the metastable well. In the first 10 ps the dephasing of the components of the wave packet is sufficiently weak that the dominant behavior is periodic. However, the amplitude of the wave packet decreases each time R_x is reached by virtue of leakage to the ground-state potential energy surface and dissociation to form Na + I. After 10 ps the dephasing and rephasing of the wave packet and the accompanying leakage to the ground-state potential energy surface dominate the dynamics, with the interval 10 ps $< t <$ 17 ps most clearly displaying the multiple periodic character of the evolution of the superposed states and the period 17 ps $< t <$ 33 ps displaying the behavior of the rephased wave packet. The associated cumulative flux $J_f(t)$ clearly displays step increases in the early stages of the evolution of the wave packet, but these are washed out as time increases. The conditions on dephasing and rephasing of the wave packet in the long time dynamics of NaI after excitation has been examined previously.[11,13]

When the pump pulse is chirped, the behavior of $P_I(t)$ and $J_f(t)$ are different from that just described. As shown in Figure 2c, for the linear chirp $\alpha = 5 \times 10^{-6}$, the interval over which $P_I(t)$ displays simple periodic character is shortened to approximately 5 ps, but the period remains about the same as in the absence of chirp. Dephasing and rephasing of the wave packet are still evident in $P_I(t)$, but the amplitude of the wave packet is, in general, less than in the absence of chirp. With this pump pulse, step increases in $J_f(t)$ are only evident in the first 3 ps of the evolution of the wave packet. The yield of Na + I is almost the same for the unchirped and chirped pump pulses (slightly less when the chirped pump pulse is used). A comparison of the cumulative fluxes generated by equal magnitude positively and negatively chirped pulses ($\alpha_{pos} = -\alpha_{neg}$) shows that the sign of the chirp has little effect on the product yield.

Figure 3a, displays $P_I(t)$, and Figure 3c displays $J_f(t)$, for the case that the pump pulse is unchirped and chirped, both with fwhm of 62 fs. When the pump pulse is not chirped (Figure 3a), $P_I(t)$ is periodic for the full 40 ps the calculation covers. However, the envelope of $P_I(t)$ does not decay exponentially. When the pump pulse is chirped (Figure 3b), the simple oscillatory character of $P_I(t)$ disappears after about 5 ps and reappears after about 17 ps. The two pump pulses generate very nearly the same product yield (Figure 3c). The source of the difference between the dynamics generated by these pump pulses is the difference in their spectral widths. A pulse with nonzero chirp has a larger spectral width than does the corresponding unchirped pulse, hence also has smaller temporal width. We have already seen, in the case of the 21 fs pump pulse, changes in the wave packet dynamics that are similar to those displayed in Figure 3b.

Figure 4a, displays $P_I(t)$, and Figure 4c displays $J_f(t)$, for the case that the pump pulse is unchirped and chirped, both with fwhm of 186 fs. This pulse width is close to that employed in the experimental studies of Jouvet et al. When the pump pulse is not chirped (Figure 4a), $P_I(t)$ is periodic for the full 40 ps the calculation covers, and in this case, the envelope of $P_I(t)$ does decay exponentially. When the pump pulse is chirped (Figure 4b), the simple oscillatory character of $P_I(t)$ disappears after about 4 ps and reappears after about 20 ps. Moreover, in this case the yield of free atoms generated by the chirped pulse is 2.5-fold greater than that generated by the unchirped pulse. Indeed, the amplitudes of $P_I(t)$ and $J_f(t)$ also increase as the pulse width increases, which is consistent with the pulse area theorem.

The calculations just described provide an explanation for the difference between the results of the experimental studies of Jouvet et al. and of Cong et al.; the former "do not observe a chaotic regime between 10 and 20 ps", while the latter do.

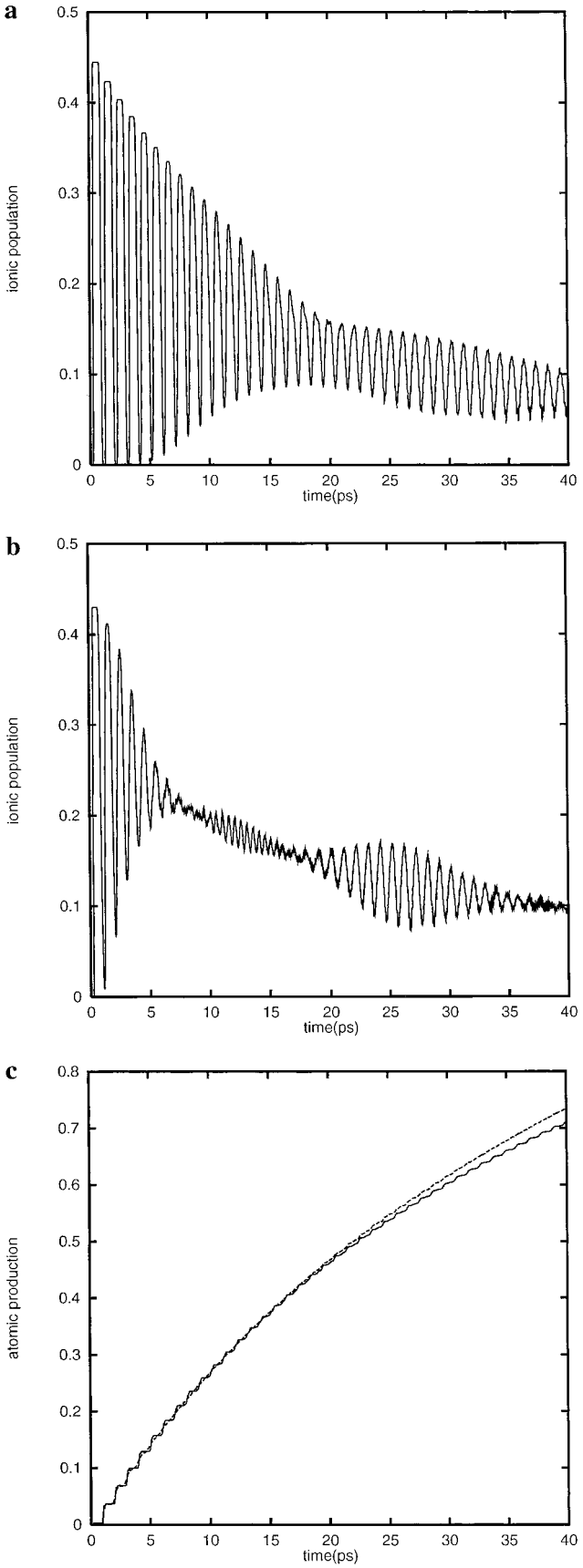

Figure 3. (a) Ionic-state population generated by an unchirped pulse of width 62 fs. (b) Ionic-state population generated by a chirped pulse with $\alpha = 10^{-6}$. (c) Atomic production $J_f(t)$. The solid line is for an unchirped pump pulse; the dashed line for a chirped pump pulse with $\alpha = 10^{-6}$.

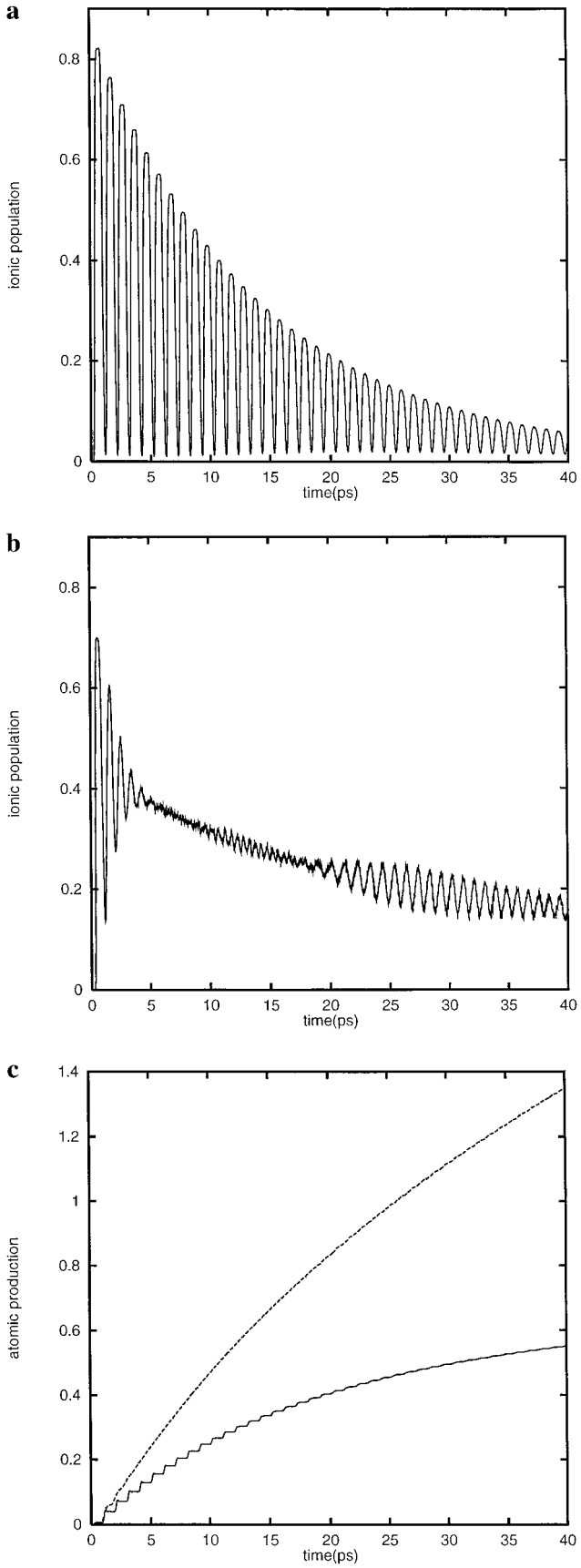

Figure 4. (a) Ionic-state population generated by an unchirped pulse of width 186 fs. (b) Ionic-state population generated by a chirped pulse with $\alpha = 10^{-6}$. (c) Atomic production $J_f(t)$. The solid line is for unchirped pump pulse; the dashed line for a chirped pump pulse with $\alpha = 10^{-6}$.

This difference can be traced to the quite different pump pulse widths that are used in the respective experiments: Jouvet et al. employed pump pulses that, at different central wavelengths, had fwhm of 120−175 fs and 250−300 fs, while Cong et al.

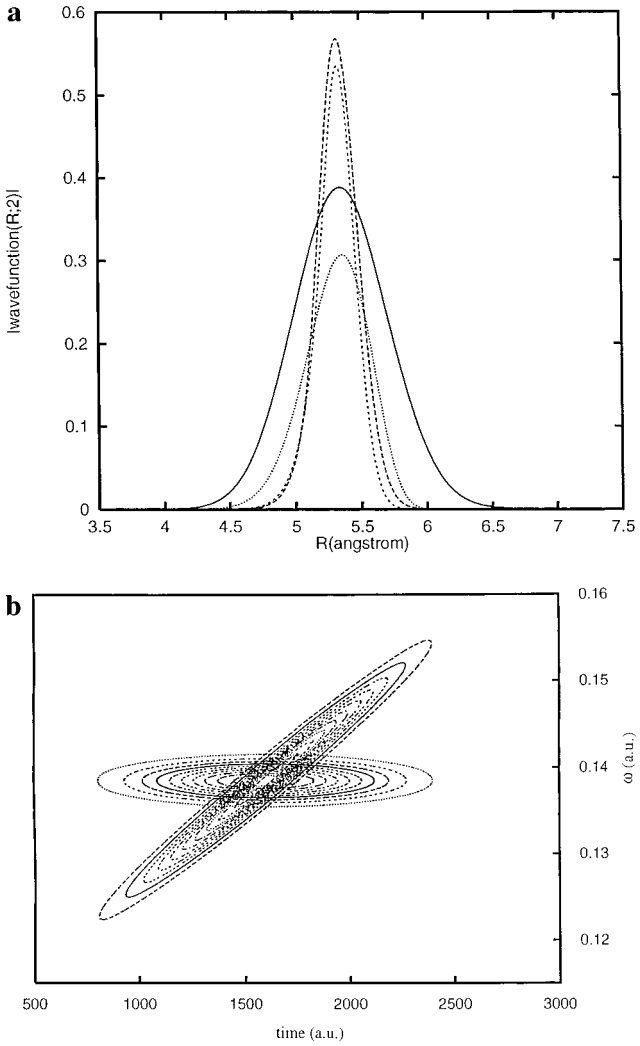

Figure 5. (a) Wave function profiles for states generated by an unchirped pulse and by several positively chirped pulses. Unchirped pulse (—); $\alpha = 5 \times 10^{-6}$ (- - -); $\alpha = 10^{-5}$ (- - -); $\alpha = 2 \times 10^{-5}$ (···). (b) Wigner transform contour plot for an unchirped pulse and the best linearly chirped pulse.

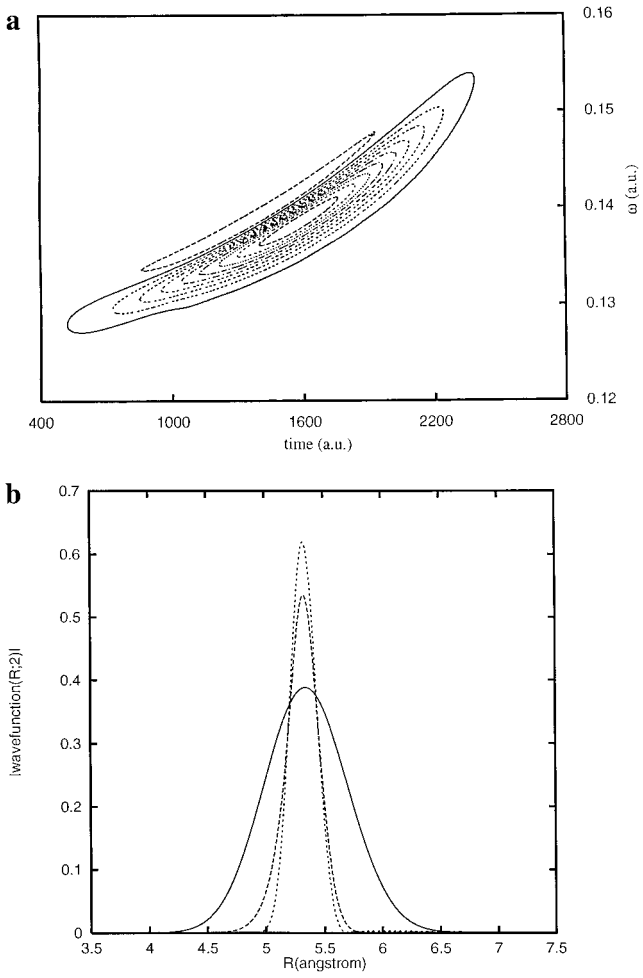

Figure 6. (a) Wigner transform contour plot for the optimum chirped pulse. (b) Wave function profiles for states generated by an unchirped pulse (—); the best linear chirped pulse (- - -); the optimal chirped pulse (···).

employed a pump pulse with fwhm of 50−60 fs. The shorter pulse creates a wave packet with a broader energy distribution in the upper state, which then dephases more rapidly. A pump pulse with fwhm of 186 fs only excites very few vibrational states; hence the probabilistic character of the Landau−Zener leakage to form Na and I on the ground-state potential energy surface is expected to generate an exponential decay of the envelope of $P_l(t)$.

It is worthy of pointing out that our calculation results on $P_l(t)$ and $J_f(t)$ at 21 fs unchirped pulse, or at 62 fs chirped pulse, resemble the experimental results of Cong et al. at 60 fs excitation pulse. The speculated reason may be 2-fold. On the theoretical side, the potential surfaces utilized in the calculations may not be accurate enough, the transition dipole moment likely has a coordinate-dependent distribution, and the assumptions on the observables used to simulate fluorescence data without explicit invocation of a third surface are not sufficiently accurate. On the experimental side, the pulses used in the lab may indeed bear the signature of chirp because of the lack of the sufficient postcompensation optical sequences during pulse generation.

B. Controlled Localization of a Wave Packet. We now examine the extent of control of the localization of a vibrational wave packet on an excited-state potential energy surface which can be achieved with a chirped pump pulse.

We consider first the evolution of the wave packets generated on the first excited state of NaI by a Gaussian pulse and by several positively chirped pulses, all with fwhm of 21 fs. Figure 5a displays those wave packets 110 fs after excitation, at which time the centers are located in the region $R = 5.3-5.4$ Å. By obtaining the wave packets generated by several negatively chirped pulses with the same fwhm, we conclude that a negatively chirped pump pulse produces a less localized wave packet than does a positively chirped pulse. A positively chirped pump pulse can be expected to generate better wave packet localization than a negatively chirped pump pulse because, during the first half of the pulse, the amplitude placed on the excited-state potential energy curve will, in general, acquire outgoing momentum at the inner turning point of the potential energy curve. Then, in order that the amplitude placed on the excited-state potential energy curve during the second half of the pulse overlaps with the amplitude already present, it must be created with sufficient outgoing momentum, which is achieved by increasing the excitation energy so that the inner turning point occurs higher on the repulsive wall of the potential energy curve, i.e., endowing the pump pulse with a positive chirp. The Wigner transforms,[34,35]

$$W(t,\omega) = \frac{1}{\pi\hbar}\int d\tau E^*(t+\tau)\, E(t-\tau) e^{2i\omega\tau} \qquad (23)$$

of the unchirped and the best of the linearly chirped pump pulses are shown in Figure 5b.

An examination of the ground and first excited state potential energy curves of NaI reveals that linear chirping of the pump pulse is not sufficient to generate optimum localization of the wave packet. To determine the chirp that produces the best localization, we used optimal control theory (see section II). For the case under consideration, the target wave packet was a delta function whose momentum was that of the propagating wave function obtained from the best linear chirp field. The Wigner transform of the optimum chirped pulse is displayed in Figure 6a; the results clearly show that the optimum pulse has a nonlinear chirp. The wave packet localization from optimum chirp pulse is shown in Figure 6b. We note that the improvement in wave packet localization relative to that achieved with the best linear chirp is small.

It is important to point out that our target function is different from that used by Wilson et al.[14] They sought optimum localization of a wave packet on its first return toward the inner turning point on the excited-state potential energy curve, whereas we have sought optimum localization of a wave packet with outgoing momentum. The optimum chirps required to generate these target functions are different, negative in the former case and positive in the latter case.

IV. Conclusions

We have reexamined the excitation dynamics and the control of the branching between photodissociation products of NaI when irradiated with pulses of various duration (hence also varying spectral width). We have resolved the apparent discrepancy between those experiments that employ relatively short pulses (50−60 fs) and those that employ relatively long pulses (150−175 fs). The wave packet dynamics generated by different width pulses can be quite different by virtue of the distribution of vibrational states on the excited-state surface that is created by the pump pulses. We have also shown that chirped pulses can dramatically improve the yield of I in the photodissociation of NaI; in one case, the use of a chirped pulse increased the product yield by a factor of 2.5.

Acknowledgment. This research was supported by a grant from the National Science Foundation.

References and Notes

(1) Rose, T. S.; Rosker, M. J.; Zewail, A. H. *J. Chem. Phys.* **1989**, *91*, 7415.

(2) Cong, P.; Mokhtari, A.; Zewail, A. H. *Chem. Phys. Lett.* **1990**, *172*, 109.

(3) Herek, J. L.; Materny, A.; Zewail, A. H. *Chem. Phys. Lett.* **1994**, *228*, 15.

(4) Cong, P.; Roberts, G.; Herek, J. L.; Mokhtari, A.; Zewail, A. H. *J. Phys. Chem.* **1996**, *100*, 7832.

(5) Jouvet, C.; Martrenchard, S.; Solgadi, D.; Dedonder-Lardeux, C.; Mons, M.; G. Gregoire, Dimicoli, I.; Piuzzi, F.; Visticot, J. P.; Mestdagh, J. M.; D'Oliveira, P.; P. Meynadier Perdrix, M. *J. Phys. Chem.* **1997**, *101*, 2555.

(6) Knopp, G.; Schmitt, M.; Materny, A.; Kiefer, W. *J. Phys. Chem.* **1997**, *101*, 4852.

(7) Engel, V.; Metiu, H. *J. Chem. Phys.* **1989**, *90*, 6116.

(8) Engel, V.; Metiu, H. *Chem. Phys. Lett.* **1989**, *155*, 77.

(9) Engel, V.; Metiu, H.; Almeida, R.; Marcus, R. A.; Zewail, A. H. *Chem. Phys. Lett.* **1988**, *152*, 1.

(10) Metiu, H.; Engel, V. *J. Opt. Soc. Am. B* **1990**, *7*, 1709.

(11) Ch. Meier, Engel, V.; Briggs, J. S. *J. Chem. Phys.* **1991**, *95*, 7337.

(12) Choi, S. E.; Light, J. C. *J. Chem. Phys.* **1989**, *90*, 2593.

(13) Chapman, S.; Child, M. S. *J. Phys. Chem.* **1991**, *95*, 578.

(14) Bardeen, C. J.; Che, J.; Wilson, K. R.; Yakovlev, V. V.; Cong, P.; Kohler, B.; J. L. Krause Messina, M. *J. Phys. Chem.* **1997**, *101*, 3815.

(15) Braun, M.; Meier, C.; Engel, V. *J. Chem. Phys.* **1996**, *105*, 530.

(16) Tang, H.; Kosloff, R.; Rice, S. A. *J. Chem. Phys.* **1994**, *101*, 8737.

(17) Hiller, E. M.; Cina, J. A. *J. Chem. Phys.* **1996**, *105*, 3419.

(18) Gross, P.; Neuhauser, D.; Rabitz, H. *J. Chem. Phys.* **1992**, *96*, 2834.

(19) Balakrishnan, N.; Kalyanaraman, C.; Sathyamurthy, N. *Phys. Rep.* **1997**, *280*, 79.

(20) Kosloff, R.; Rice, S. A.; Gaspard, P.; Tersigni, S.; Tannor, D. J. *Chem. Phys.* **1989**, *139*, 201.

(21) Amstrup, B.; Carlson, R. J.; Matro, A.; Rice, S. A. *J. Phys. Chem.* **1991**, *95*, 8019.

(22) Ruhman, S.; Kosloff, R. *J. Opt. Soc. Am. B* **1990**, *7*, 1748.

(23) Amstrup, B.; Doll, J. D.; Sauberbrey, R. A.; Szabo, G.; Lorincz, A. *Phys. Rev. A* **1993**, *48*, 3830.

(24) Melinger, J. S.; Hariharan, A.; Gandhi, S. R.; Warren, W. S. *J. Chem. Phys.* **1991**, *95*, 2210.

(25) Melinger, J. S.; Gandhi, S. R.; Hariharan, A.; Goswami, D.; Warren, W. S. *J. Chem. Phys.* **1994**, *101*, 6439.

(26) Sterling, M.; Zadoyan, R.; Apkarian, V. A. *J. Chem. Phys.* **1996**, *104*, 6497.

(27) Paloviita, A.; Suominen, K.-A.; Stenholm, S. *J. Phys. B* **1993**, *28*, 1463. Paloviita, A. *Opt. Commun.* **1995**, *119*, 533.

(28) Lai, W. K.; Suominen, K.-A.; Garraway, B. M.; Stenholm, S. *Phys. Rev. A* **1993**, *47*, 4779.

(29) Suominen, K.-A.; Garraway, B. M. *Phys. Rev. A* **1993**, *48*, 3811.

(30) Cerullo, G.; Bardeen, C. J.; Wang, Q.; Shank, C. V. *Chem. Phys. Lett.* **1996**, *262*, 362.

(31) Arfken, G.; *Mathematical Methods for Physicists*, 3rd ed.; Academic Press Inc.: New York, 1985; p 803.

(32) Shank, C. V. In *Ultrashort Laser Pulses and Applications*; Kaiser, W., Ed.; Springer -Verlag: Berlin, 1988.

(33) Landau, L. D.; Lifshitz, E. M. *Quantum Mechanics*; Pergamon Press Ltd.: New York, 1965.

(34) Hillery, M.; O'Connell, R. F.; Scully, M. O.; Wigner, E. P. *Phys. Rep.* **1984**, *106*, 121.

(35) Paye, J. *IEEE J. Quantum Electron.* **1992**, *28*, 2262.